Time Of Flight Image Sensors in 0.18µm CMOS Technology: a Comparative Overview of Different Approaches

David Stoppa[a], Lucio Pancheri[a], Nicola Massari[a], Mattia Malfatti[a], Matteo Perenzoni[a], Gianmaria Pedretti[a], Gian-Franco Dalla Betta[b]

[a]*Fondazione Bruno Kessler, Via Sommarive 18, 38123 Trento, Italy*
[b]*DISI, University of Trento, Via Sommarive 14, 38123 Trento, Italy*
phone: +39 0461 314531, e-mail: stoppa@fbk.eu

Abstract

In this paper a comparative review of three image sensors fabricated in a 0.18µm CMOS imaging technology [1-3] and conceived for TOF range imaging is given. Two of them exploit in-pixel electro-optic demodulating detectors, while the third one is based on a switched capacitor pixel approach using a standard photodiode.

Introduction

Time of Flight (TOF) range cameras, besides being used in industrial metrology applications, have also a potential interest in consumer application such as ambient assisted living and gaming. In these fields, the information offered by the sensor can be used to efficiently track the position of objects and people in the camera field of view, thus overcoming many of the problems, which are present when analyzing conventional intensity images. The need of lowering the overall system cost and power consumption, while increasing the sensor resolution, has triggered the exploration of more advanced CMOS technologies to make sensors suitable for these applications. However, migration to new technologies is not straightforward, since the most mature commercial 3D sensors employ dedicated CCD-CMOS technologies, which cannot be translated to new processes without any process modification. In this contribution a comparative overview of three different pixel architectures aimed at TOF 3D imaging, and implemented in the same 0.18-µm CMOS technology, is given and the main advantages and drawbacks of each solution are analyzed.

Demodulating Detectors Approach

The working principle of a typical TOF imaging system [4] is shown in Fig. 1: the phase delay of a modulated or pulsed light back-scattered by the objects in the observed scene is measured by each pixel of the array and the distance is calculated from this delay. In the first array (sensor A) a buried-channel photonic demodulator was designed using imaging technology-specific layers (Fig. 2). The two outputs of the pixel are read-out using standard active pixel readout electronics with the addition of a global shutter and anti-blooming transistor (Fig. 3). This pixel can perform homodyne demodulation in the charge domain, and the difference between the two outputs contains information about the phase delay. The device exhibits a good demodulation contrast also at frequencies exceeding 50MHz (Fig. 4). The second solution implemented (sensor B) is based on a Current Assisted Photonic Demodulator (CAPD) [2],[5] as light sensing and mixing devices (Fig. 5). While using a different photo-demodulator device, the pixel electronics is similar to the one used in sensor A. Also in this case (Fig. 6) a high demodulation contrast has been achieved beyond 50 MHz, but an efficient demodulation requires a large modulation current of 400mA for the whole array.

Switched Capacitor Pixel Approach

The third solution belongs to the category of sensors based on an extensive use of electronics in the pixel, which typically require pixel pitch beyond 100µm, making them impracticable for realization of large two-dimensional pixel arrays [6-8]. Fig. 7 shows the schematic of the sensor C pixel, which is composed by a current integrator and a switched capacitor voltage accumulator. The first stage output voltage can be sampled and transferred to C2, with '+' or '-' sign, using signals FWD and BWD. This structure allows performing CDS, integrated pulse accumulation, and also background light subtraction. To reduce the impact of the second stage input offset the amplifier is implemented as a folded cascode with a 4-bit offset compensation circuitry. The resulting pixel pitch is of 29.1µm with a fill factor of 34%. The chip can also operate as a high sensitivity and high frame rate image sensor with in-pixel CDS (Fig. 8).

Distance Measurements and 3D Imaging Capabilities

Fig. 9 shows the sensors noise as a function of the target (white plane) distance taken at different frame rates and also normalized to allow a frame-rate independent comparison. Consecutive frames taken at video rate are shown in Fig. 10 while Fig. 11 summarizes the main characteristics and performance of the three sensors.

COMPARATIVE OVERVIEW AND CONCLUSIVE REMARKS

Sensors A and B exhibit similar performance in terms of demodulation contrast and maximum demodulation frequency, however, sensor B suffers from very high power consumption due to the modulation voltage applied over a very low equivalent resistance, which limits its implementation within large pixel array. Moreover, although in this implementation the two pixels have the same fill factor - we decided to share the very same pixel structure for a direct comparison of the performance - sensor A could potentially achieve higher fill factor because the two modulation lines can be designed by using minimum metal width. On the other hand, sensor B has higher quantum efficiency at lower wavelengths because there is no polysilicon gate on the top of the active area. This is not a big issue in TOF applications, where IR light is always used, but limits the exploitation of such a sensor in other applications domains where shorter wavelengths are needed (e.g. fluorescence lifetime imaging).

Another key point is that sensor A requires a detailed knowledge of the process fabrication steps to be successfully ported to other CMOS technologies, and the fully compatibility with other standard technologies is not guaranteed. On the contrary, the implementation of sensor B in other CMOS technologies is straightforward and reliable, although the availability of relatively low-doped and epitaxial substrates improves the sensor performance. An important aspect concerning the design of sensor B is the proper layout of the collection junctions and of the p-well implant connected to ground surrounding the device active area. Those parameters will affect the shape of the electric field into the substrate with a major impact onto the demodulation contrast and the sensor power consumption.

Both sensors A and B are immune to low-intensity background light, because of the differential pixel read out, but this is true only if none of the two pixel outputs saturates. In fact, both modulated light echo and stray light are integrated for the same exposure time, thus limiting the rejection of uncorrelated continuous signals. This is a common problems of in-pixel demodulating-detectors, which can be attenuated by means of charge draining structures [9] and the use of interferometric filters tuned on the modulated light wavelength. On the contrary, pulsed-light technique provides much better immunity to background light [3,8] , mainly for two reasons: (i) there is an intrinsic concentration of the signal energy into a train of short light bursts so that, by properly timing the sensor exposure in a lock-in operation mode, uncorrelated light is filtered out (as the ratio of the pulse width over the single-exposure time); (ii) double differential exposures operation can be implemented, where the illuminator is active only in the first integration, so that continuous light is removed at each detected pulse echo. Because of that sensor C is immune to background light up to 20klux without the need of any filter. However, SC charge accumulation prevents the use of a large number of pulses (typically around 128), and the much more complex in-pixel electronics adds also significant noise, making the precision of those kind of sensors generally worst with respect to the photodemodulator-detector approach. Ultimately, the pixel structure of sensor C with respect to A and B is much more complex thus limiting the minimum pixel pitch and the pixel power consumption performance. As a summary, sensors A and B are the best candidate for consumer market applications (indoor operation, large spatial resolution, low system cost) while sensor C is more suitable for security and automotive (uncontrolled light and temperature environment).

ACKNOWLEDGMENTS

This work has been supported by the European Community 6-th Framework Programme within the project NETCARITY (http://www.netcarity.org/).

REFERENCES

[1] D. Stoppa et al., “A Range Image Sensor Based on 10-µm Lock-In Pixels in 0.18µm CMOS Imaging Technology”, IEEE J. of Solid-State Circuits, Vol. 46(1), pp. 248-258, 2011.

[2] L. Pancheri et al., “A 120x160 pixel CMOS range image sensor based on current assisted photonic demodulators”, Proc. SPIE Vol. 7726, 772615, 2010.

[3] M. Perenzoni et al., “A 160×120-Pixels Range Camera with On-Pixel Correlated Double Sampling and Non-uniformity Correction in 29.1µm pitch”, Proc. IEEE ESSCIRC 2010, Seville, Spain, 13-17 Sept. 2010.

[4] B. Hosticka, P. Seitz, A. Simoni, “Optical time-of-flight sensors for solid-state 3D-vision”, Encyclopedia of Sensors, Vol. 7, pp. 259-289, 2006.

[5] W. van derTempel, et al., “A 1k-pixel 3D CMOS sensor”, Proc. of IEEE Sensors Conference, pp. 1000-1003, Oct. 2008.

[6] O. Elkhalili, et al., “A 4x64 pixel CMOS image sensor for 3-D measurements applications”, IEEE J. Solid-State Circuits, vol. 39, no. 7, pp. 1208-1212, Jul. 2004.

[7] G. Zach, et al., “Extraneous-light resistant multipixel range sensor based on a low-power correlating pixel-circuit”, Proc. of the 35th IEEE ESSCIRC’09, pp. 236-239, Sept. 2009.

[8] D. Stoppa, et al., “A 16x16-pixel range-finding CMOS image sensor”, Proc. of the 30th IEEE ESSCIRC’04, pp. 419-422, Sept. 2004.

[9] S. Kawahito, et al., “A CMOS time-of-flight range image sensor with gates-on-field-oxide structure”, IEEE Sensors J., vol. 7, no. 12, pp. 1578 – 1586, Dec. 2007.

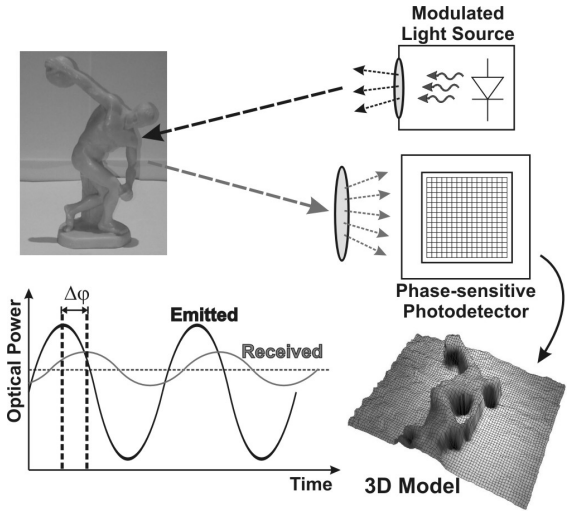

Figure 1. Time-of-flight measurement setup.

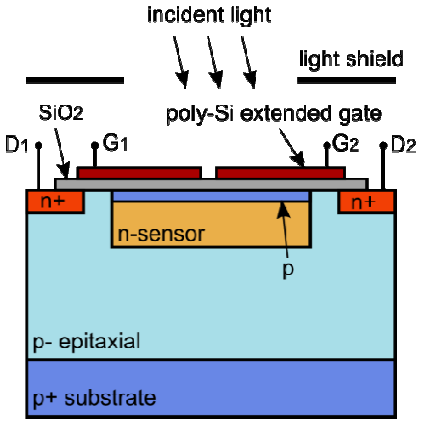

Figure 2. Cross-section of the buried-channel photonic demodulator.

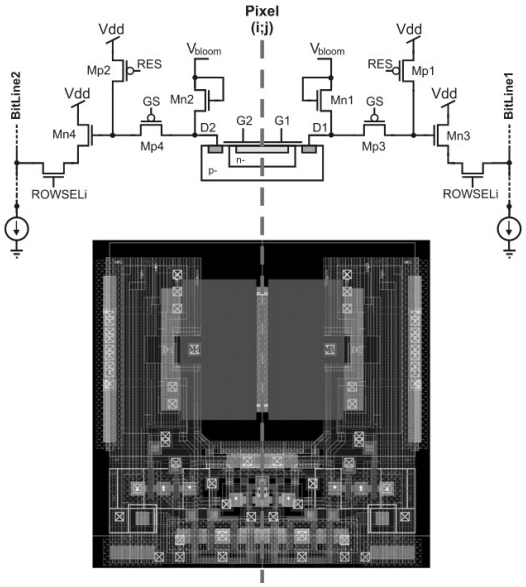

Figure 3. Pixel schematic diagram and layout.

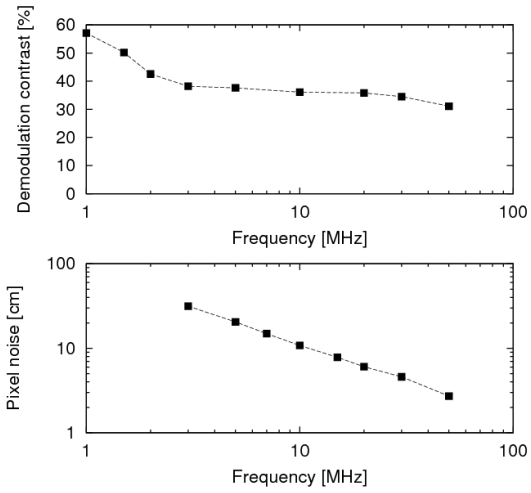

Figure 4. Demodulation contrast of buried-channel demodulator pixel and projected pixel noise as a function of modulation frequency.

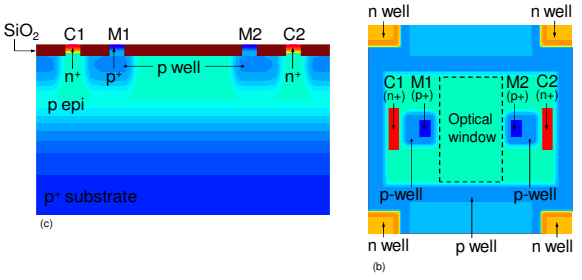

Figure 5. Cross-sectional view (a) and top view (b) of the CAPD pixel.

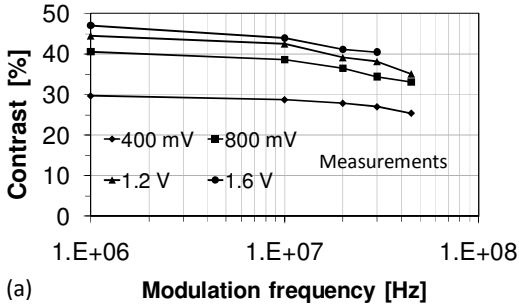

Figure 6. Experimental demodulation contrast of CAPD pixel as a function of modulation frequency for different modulation signal amplitudes.

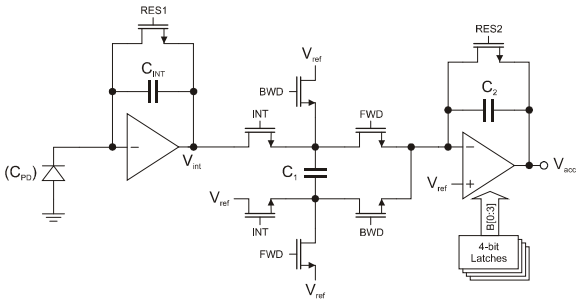

Figure 7. Schematic of the proposed two-stage pixel with offset correction.

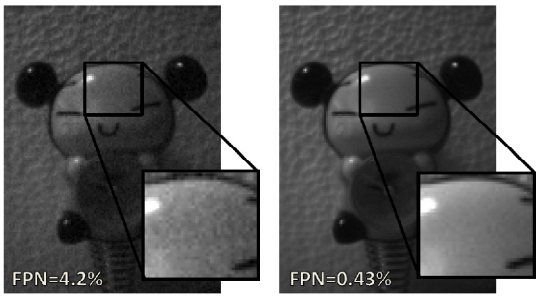

Figure 8. Picture taken at 458 fps (T_{int}=200µs, 10MS/s) without (left) and with 4-bit FPN correction (right).

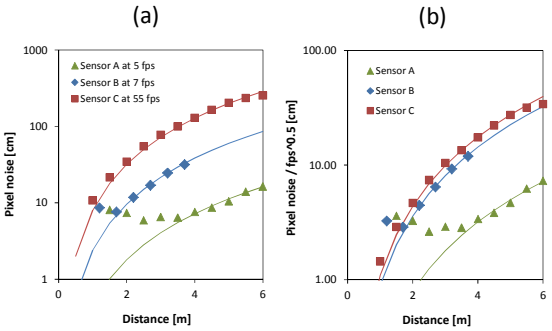

Figure 9. (a) Pixel noise for the distance measurement of a white plane target, (b) pixel noise normalized for the square root of the frame rate.

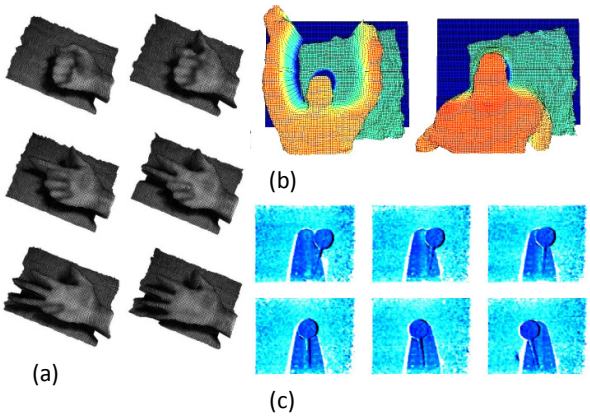

Figure 10. Frames extracted from video acquisitions using (a) sensor A at 10 fps (b) sensor B at 7 fps and (c) sensor C at 70 fps .

	Parameter	Sensor A	Sensor B	Sensor C
Sensor	Detector	Buried Channel Demodulator	CAPD	n-well photodiode
	Supply voltage	1.8 V, 3.3 V	1.8 V, 3.3V	1.8 V
	Current consumption	4mV from 1.8V 14 mV from 3.3V	400mA (mainly due to modulation current)	175 mA
	Array size [pixels]	80x60	160×120	160×120
	Pixel pitch	10µm	10µm	29.1 µm
	Fill-factor	24 %	24 %	34 %
	Dynamic range	51 dB	51 dB	50 dB
3D Camera System	Illuminator type	LED 850nm	LED 850nm	Pulsed Laser 905nm
	Modulation frequency	20 MHz	20 MHz	-
	Laser pulse width	-	-	50ns
	Laser repetition rate	-	-	15kHz max
	Illuminator optical power (total on the scene)	80mW	140mW	44mW(at 55fps)
	Objective	f = 6mm, F# = 1.4	f = 2.9mm, F# = 1	f=12.5mm, F# = 1.3
	Max frame rate	30 fps	10 fps	80 fps
	Best precision	<4 cm	<10 cm	10 cm

Figure 11. Comparative performance summary table.